Hybrid Finite-Element Analysis of Electromagnetic Plane Wave Scattering from Axially Periodic Cylindrical Structures

Angelo Freni, *Member, IEEE,* Christos Mias, *Member, IEEE,* and Ronald L. Ferrari

***Abstract*— In many antenna systems the primary feed or the subreflector will most often be supported by struts which obstruct the aperture and therefore cause a reduction in the directivity and an increase in sidelobe levels. So as to be able to design new structures which avoid these drawbacks, the problem of plane wave scattering from an infinite axially periodic cylinder of arbitrary geometric and material parameters is analyzed in this paper by a hybrid finite element/boundary element method. Covariant-projection edge elements are employed in the inhomogeneous region of the unit cell and the scattered field is expanded in terms of cylindrical Floquet harmonics. The resulting practical numerical procedure has been tested to ensure that power conservation rules are obeyed and checked satisfactorily against both analytical results and measurements on periodically loaded struts.**

***Index Terms*—Boundary element method, cylinder, electromagnetic scattering by periodic structure, finite-element method.**

I. Introduction

In antenna systems there are many situations where the electromagnetic waves are obstructed by a mechanical structure causing an increase in the sidelobes and a reduction in gain. This problem arises especially when compact antennas are designed.

The mechanical structure often consists of one or more rods (i.e., feed support struts in axisymmetric reflector antennas or the framework of a space frame radome), that are shaped and loaded in such a way that the blockage is minimized.

The blockage effect of simple uniform cylindrical struts and masts of different cross sections has been widely analyzed [1]–[3]. However, in recent years new structures have been designed in order to minimize this negative effect. This has been done by appropiately shaping the structure and by making it nonuniform in the axial direction in a way similar to that adopted to create artificially "hard" surfaces [4]. The considerable improvements reported are very promising [5]–[7].

Due to the complexity of the problem, so far only a few simple cases of a corrugated axially symmetric cylinder have been studied [8]–[11].

Manuscript received January 28, 1997; revised June 16, 1997.

A. Freni is with the Department of Electronic Engineering, University of Florence, I-50139 Florence, Italy.

C. Mias is with the School of Electronic and Electrical Engineering, The University of Birmingham, Birmingham, B15 2TT, U.K.

R. L. Ferrari is with the Engineering Department, Cambridge University, Cambridge, CB2 1PZ, U.K.

Publisher Item Identifier S 0018-926X(98)09713-0.

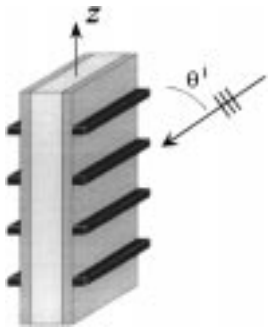

Fig. 1. Geometry of the problem.

In this paper, a hybrid technique which utilizes a finite element/boundary element method (FEM-BEM) is presented to analyze the scattering of an electromagnetic plane wave obliquely incident upon an axially periodic cylinder of arbitrary geometric and material parameters. This provides a useful tool for the study of new struts and masts. In particular, the complex periodic structure is analyzed by using a Galerkin weighted residual finite-element method (FEM) employing three-dimensional covariant-projection elements [12]: curvilinear bricks which impose only tangential field continuity and work well even when sharp metal edges are present. The periodicity of the structure has been properly taken into account using periodic weight functions while the radiation condition has been imposed through expanding the field in the free space surrounding the structure in terms of cylindrical Floquet harmonics. Numerical results of different corrugated structures, for both TE_z and TM_z polarized incident fields are shown and validated as far as is possible.

II. Formulation

The geometry of an infinitely long cylinder having axis parallel to the z-axis of the cylindrical coordinate system (ρ, ϕ, z) and periodicity D_z with respect to the z direction is shown in Fig. 1. We assume that the surrounding medium is free space with permittivity ϵ_0 and permeability μ_0. The direction of the incident plane wave makes an angle θ^i with the positive z-axis and is parallel to the xz-plane. A harmonic time dependence $\exp(j\omega t)$ is assumed and suppressed.

Since the incident wave is a plane wave and the geometry of the scatterer is a periodic function of z with period D_z, the fields observed at two arbitrary points, separated by a distance D_z along a line parallel to the z-axis, are identical except for a constant phase shift $\exp(jk_0 D_z \cos\theta^i)$. This means that it

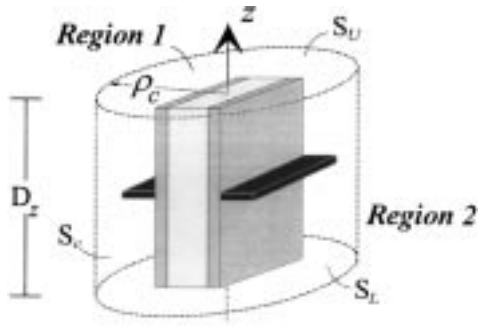

Fig. 2. Unit periodic cell.

is necessary to determine the scattered field only in a basic period $-D_z/2 \le z \le D_z/2$.

In particular, we can partition each basic period into two regions (Fig. 2). Region 1 extends to envelope the periodic structure and is delimited by a circular cylindrical surface S_c of radius ρ_c concentric with the z-axis. Region 2 consists just of free space surrounding the periodic structure. In Region 1 we solve the electromagnetic problem applying a Galerkin weighted residual finite element formulation, based on covariant-projection vector elements, while in Region 2 the field is represented in terms of a double series of cylindrical Floquet harmonics.

Since the medium that surrounds the corrugated cylinder is homogeneous, we can express the fields in terms of transverse electric and transverse magnetic potentials. Each of these two potentials must satisfy the Helmholtz equation, in scalar form, subject to the periodic boundary conditions. This equation can easily be solved using the standard method of separation of variables with application of the periodicity conditions as similarly described in [13]. Taking into account the different form of the separated differential equations for propagating and evanescent modes, the components of the scattered field tangential to the cylindrical surface S_c can be expressed as

$$\begin{bmatrix} E_\phi^s \\ E_z^s \end{bmatrix} = \sum_{m=-\infty}^{\infty} \sum_{n=-\infty}^{\infty} \Phi_{mn}(\phi, z) \cdot \begin{bmatrix} \dfrac{j\omega\mu_0}{\eta_n k_{\rho_n}} R'_{mn}(\rho) & \dfrac{-mk_{z_n}}{\rho\eta_n k_{\rho_n}^2} R_{mn}(\rho) \\ 0 & R_{mn}(\rho) \end{bmatrix} \begin{bmatrix} a_{mn}^{\mathrm{TE}} \\ a_{mn}^{\mathrm{TM}} \end{bmatrix} \tag{1}$$

$$\begin{bmatrix} H_\phi^s \\ H_z^s \end{bmatrix} = \sum_{m=-\infty}^{\infty} \sum_{n=-\infty}^{\infty} \Phi_{mn}(\phi, z) \cdot \begin{bmatrix} \dfrac{-mk_{z_n}}{\rho\eta_n k_{\rho_n}^2} R_{mn}(\rho) & \dfrac{-j\omega\epsilon_0}{\eta_n k_{\rho_n}} R'_{mn}(\rho) \\ R_{mn}(\rho) & 0 \end{bmatrix} \begin{bmatrix} a_{mn}^{\mathrm{TE}} \\ a_{mn}^{\mathrm{TM}} \end{bmatrix} \tag{2}$$

where a_{mn}^{TE} and a_{mn}^{TM} are unknown transverse electric and magnetic constants, respectively, and

$$k_{z_n} = k_0 \cos\theta^i + \frac{2n\pi}{D_z} \tag{3}$$

$$k_{\rho_n}^2 = |k_0^2 - k_{z_n}^2| \tag{4}$$

$$\eta_n = \mathrm{sign}(k_0^2 - k_{z_n}^2) \tag{5}$$

while $k_0 = \omega\sqrt{\epsilon_0\mu_0}$ is the propagation constant of free space. Furthermore,

$$\Phi_{mn}(\phi, z) = \exp(jm\phi)\exp(jk_{z_n} z) \tag{6}$$

and

$$R_{mn}(\rho) = \begin{cases} H_m^{(2)}(k_{\rho_n}\rho), & \text{for } k_0^2 > k_{z_n}^2 \\ K_m(|k_{\rho_n}|\rho), & \text{for } k_0^2 < k_{z_n}^2 \end{cases} \tag{7}$$

where $H_m^{(2)}$ and K_m are the Hankel function and the modified Bessel function of the second kind, respectively, and $R'_{mn}(\rho)$ indicates the derivative of these functions with respect to the argument $k_{\rho_n}\rho$. The choice of two different forms for the $R_{mn}(\rho)$ function corresponds to the physics of the wave harmonics, either propagating or evanescent, and allows an easier and more efficient numerical evaluation of the solution.

In Region 1, we need to solve the wave equation subject to appropriate boundary conditions. In particular these are the continuity of the tangential components of the electric and magnetic field on surface S_c and the periodicity of the field along the z direction. To solve the wave equation, a finite-element procedure is applied which uses weighted residuals. For the specific configuration, the weak form of the wave equation can be written as [14]

$$\begin{aligned} &\int_V \left[(\nabla \times \vec{W}) \cdot \left(\frac{1}{\mu_r} \nabla \times \vec{E} \right) - k_0^2 \vec{W} \cdot \epsilon_r \vec{E} \right] dV \\ &\quad - \int_{S_U} \left(\vec{W} \times \frac{1}{\mu_r} \nabla \times \vec{E} \right) \cdot \hat{z} \, dS \\ &\quad + \int_{S_L} \left(\vec{W} \times \frac{1}{\mu_r} \nabla \times \vec{E} \right) \cdot \hat{z} \, dS \\ &\quad + j\omega\mu_0 \int_{S_c} \vec{W} \cdot (\vec{H} \times \hat{\rho}) \, dS = \mathbf{0} \end{aligned} \tag{8}$$

where $\vec{W}$ is the vector weighting function while, as shown in Fig. 2, S_U and S_L are the upper and the lower plane surfaces of Region 1, respectively, and V is the volume enclosed by these surfaces and the cylindrical surface S_c.

The Floquet theorem can be used as a constraint applied to the boundaries of a single periodic unit cell, which can thus be employed to provide the complete solution of the infinite periodic structure. The vector weighting function $\vec{W}$ is chosen from the same field interpolation polynomials as used to represent the field vector $\vec{E}$. Without loss of generality, $\vec{W}$ may be assumed to be periodic with a constant phase term equal to the conjugate of Floquet's constant phase term [15]

$$\vec{W}(z + D_z) = \vec{W}(z)\exp(-jk_0 D_z \cos\theta^i). \tag{9}$$

The advantage of choosing a weighting function of such form is that the integrals on the surfaces S_U and S_L required from (8) over any pair of periodic boundaries cancel each other out. Thus, only the periodic boundary condition needs to be imposed in the final matrix equation in order to completely take into account the contribution of surface integrals along periodic boundaries [16].

The continuity of transverse field components through the surface S_c now has to be imposed. We can express the

boundary integral on the cylindrical surface S_c which appears in (8) in terms of scattering and incident magnetic fields as

$$\begin{aligned} I_{S_c} &= j\omega\mu_0 \int_{S_c} \vec{W}\cdot(\vec{H}\times\hat{\rho})\,dS \\ &= j\omega\mu_0 \int_{S_c} \{W_\phi(H_z^i+H_z^s) - W_z(H_\phi^i+H_\phi^s)\}\,dS \end{aligned} \quad (10)$$

where H_z^i and H_ϕ^i express the transverse components of the incident magnetic field on the cylindrical surface S_c. By using (2) we can also rewrite the integral (10) in terms of the unknown coefficients a_{mn}^{TE} and a_{mn}^{TM} as

$$\begin{aligned} I_{S_c} &= j\omega\mu_0 \int_{S_c} (W_\phi H_z^i - W_z H_\phi^i)\,dS \\ &\quad + j\omega\mu_0 \sum_{m=-\infty}^{\infty}\sum_{n=-\infty}^{\infty} a_{mn}^{\mathrm{TE}} R_{mn}(\rho_c) \\ &\quad \cdot \int_{S_c} \left(W_\phi\Phi_{mn} + \frac{mk_{z_n}}{\eta_n\rho k_{\rho_n}^2} W_z\Phi_{mn}\right) dS \\ &\quad - k_0^2 \sum_{m=-\infty}^{\infty}\sum_{n=-\infty}^{\infty} \frac{a_{mn}^{\mathrm{TM}}}{\eta_n k_{\rho_n}} R'_{mn}(\rho_c) \\ &\quad \cdot \int_{S_c} W_z\Phi_{mn}\,dS. \end{aligned} \quad (11)$$

Furthermore, considering the orthogonality of the functions $\Phi_{mn}(\phi,z)$, we can express the unknown transverse electric and magnetic coefficients in terms of the unknown transverse electric field on the surface S_c as

$$\begin{aligned} a_{mn}^{\mathrm{TE}} &= \frac{-jk_{\rho_n}R'^{-1}_{mn}(\rho_c)}{2\pi\rho_c D_z\omega\mu_0} \\ &\quad \cdot \left[\eta_n(I_{E_\phi} - I_{E_\phi^i}) + \frac{mk_{z_n}}{\rho_c k_{\rho_n}^2}(I_{E_z} - I_{E_z^i})\right] \end{aligned} \quad (12)$$

$$a_{mn}^{\mathrm{TM}} = \frac{R_{mn}^{-1}(\rho_c)}{2\pi\rho_c D_z}(I_{E_z} - I_{E_z^i}) \quad (13)$$

where

$$I_{E_\phi} = \int_{S_c} E_\phi\Phi_{mn}^*\,dS \quad (14)$$

$$I_{E_\phi^i} = \int_{S_c} E_\phi^i\Phi_{mn}^*\,dS \quad (15)$$

$$I_{E_z} = \int_{S_c} E_z\Phi_{mn}^*\,dS \quad (16)$$

$$I_{E_z^i} = \int_{S_c} E_z^i\Phi_{mn}^*\,ds. \quad (17)$$

If we consider a TM$_z$ (i.e., $H_z = 0$) incident plane wave, of amplitude E_0, the integrals (15) and (17) can be solved analytically by employing a well-known addition theorem for Bessel functions, giving

$$I_{E_\phi^i} = -E_0\cos\theta^i \frac{2m\pi D_z}{k_{\rho_0}} j^m J_m(k_{\rho_0}\rho_c)\delta_{n0} \quad (18)$$

$$I_{E_z^i} = E_0\sin\theta^i 2\pi\rho_c D_z j^m J_m(k_{\rho_0}\rho_c)\delta_{n0} \quad (19)$$

where δ_{ij} is the Kroneker delta function and J_m is the Bessel function of the first kind of order m. Similarly, for a TE$_z$ (i.e., $E_z = 0$) incident plane wave, of amplitude E_0, we have

$$I_{E_\phi^i} = jE_0 2\pi\rho_c D_z j^m J'_m(k_{\rho_0}\rho_c)\delta_{n0} \quad (20)$$

$$I_{E_z^i} = 0 \quad (21)$$

where J'_m is the derivative of the Bessel function of first kind with respect to this argument.

Now, using (12) and (13) in (11), we can express the boundary integral on the cylindrical surface S_c as

$$\begin{aligned} I_{S_c} &= j\omega\mu_0(I_{W_\phi^i} - I_{W_z^i}) + \frac{j\omega\mu_0}{2\pi\rho_c D_z} \\ &\quad \cdot \sum_{m=-\infty}^{\infty}\sum_{n=-\infty}^{\infty} \{(A_{mn}I_{E_\phi^i} - B_{mn}I_{E_z^i})I_{W_\phi} \\ &\qquad - (B_{mn}I_{E_\phi^i} + C_{mn}I_{E_z^i})I_{W_z}\} \\ &\quad + \frac{j\omega\mu_0}{2\pi\rho_c D_z} \\ &\quad \cdot \sum_{m=-\infty}^{\infty}\sum_{n=-\infty}^{\infty} \{(A_{mn}I_{E_\phi} - B_{mn}I_{E_z})I_{W_\phi} \\ &\qquad - (B_{mn}I_{E_\phi} + C_{mn}I_{E_z})I_{W_z}\} \end{aligned} \quad (22)$$

where

$$I_{W_\phi} = \int_{S_c} W_\phi\Phi_{mn}\,dS \quad (23)$$

$$I_{W_\phi^i} = \int_{S_c} W_\phi H_z^i\,dS \quad (24)$$

$$I_{W_z} = \int_{S_c} W_z\Phi_{mn}\,dS \quad (25)$$

$$I_{W_z^i} = \int_{S_c} W_z H_\phi^i\,dS \quad (26)$$

and

$$A_{mn} = -j\frac{\eta_n k_{\rho_n} R_{mn}(\rho_c)}{\omega\mu_0 R'_{mn}(\rho_c)} \quad (27)$$

$$B_{mn} = +j\frac{mk_{z_n}R_{mn}(\rho_c)}{\omega\mu_0\rho_c k_{\rho_n}R'_{mn}(\rho_c)} \quad (28)$$

$$C_{mn} = -j\frac{\omega\epsilon_0}{\eta_n k_{\rho_n}}\left[\frac{R'_{mn}(\rho_c)}{R_{mn}(\rho_c)} - \left(\frac{mk_{z_n}}{k_0\rho_c k_{\rho_n}}\right)^2 \frac{R_{mn}(\rho_c)}{R'_{mn}(\rho_c)}\right]. \quad (29)$$

It is worth noting that for TM$_z$ polarization the term appearing in (22)

$$(A_{mn}I_{E_\phi^i} - B_{mn}I_{E_z^i}) = 0 \quad (30)$$

for each value of m and n.

Substituting (22) into the weak form of the wave equation (8) we can solve for the total electric field within Region 1. Furthermore, it is sufficient to substitute the electric field on the surface S_c thus determined into (12) and (13) to evaluate the coefficients a_{mn}^{TE} and a_{mn}^{TM} and then, through (1) and (2), the scattered field.

III. Numerical Implementation and Results

In order to apply the finite-element formulation in the inhomogeous region (i.e., Region 1), we have implemented a computer program which employs three-dimensional, 20-node, isoparametric, Crowley–Silvester covariant-projection elements of mixed order as described in [14]. This choice prevents spurious modes and allows a better modeling of singularities due to sharp metallic edges. Furthermore, since only tangential continuity is enforced, there is no difficulty caused by the discontinuity of the normal component of the electric field at dielectric interfaces.

To take into account the radiation condition by the boundary integral on the cylindrical surface S_c, for each intersection of a covariant-projection volume element with the surface S_c, we have defined an eight-node, isoparametric, covariant-projection surface element of mixed order. Each surface element has a local coordinate system (u, v) that is not necessarily orthogonal, but nevertheless can be used to define unitary vectors $\vec{a}_u, \vec{a}_v$, at each point [17]. After calculating the covariant components E_u, E_v one can get the vector $\vec{E}_t$ tangential to the cylindrical surface S_c by using the reciprocal vectors $\vec{a}^{\,u}, \vec{a}^{\,v}$

$$\vec{E}_t = E_u \vec{a}^{\,u} + E_v \vec{a}^{\,v}. \tag{31}$$

The trial functions for E_u, E_v are mixed-order; that is, each trial function for E_u is a polynomial of order two in v but order one in u, and similarly of order one in v and two in u for the other component.

Since we have chosen the vector weighting function $\vec{W}$ to be selected from the vector interpolation functions representing the electric field $\vec{E}$, all the integrals (14), (16), (23)–(26) involved in (22) are of the same form, namely,

$$\int_{S_c} F_i(\phi, z) h(\phi, z)\, dS, \qquad \text{with } i = \phi, z \tag{32}$$

where $h(\phi, z)$ can be either H_z^i or H_ϕ^i or Φ_{mn} or Φ_{mn}^* depending on integral under examination. Expressing the covariant components of the electric field ($\vec{F} = \vec{E}_t$) or of the vector weighting function ($\vec{F} = \vec{W}_t$), tangential to the cylindrical surface S_c, by means of f_u, f_v, the integral (32) can be rewritten as

$$\int_{S_c} [f_u(\vec{a}^{\,u} \cdot \hat{i}) + f_v(\vec{a}^{\,v} \cdot \hat{i})] h(\phi, z) \sqrt{g_{11} g_{22} - g_{12}^2}\, du\, dv, \qquad \text{with } i = \phi, z \tag{33}$$

where $g_{ij} = \vec{a}_i \cdot \vec{a}_j$ are metrical coefficients. This allows us to carry out easily and efficiently the integration on each surface element numerically, using a 25-point (5×5)Gaussian quadrature method.

A sparse-matrix conjugate gradient solver has been employed to solve the final finite-element matrix equation, which is sparse, complex, and asymmetric.

The same covariant-projection surface elements of mixed order have been employed to evaluate the coefficients a_{mn}^{TE} and $\alpha_{mn}^{\mathrm{TM}}$ after the electric field on the surface S_c has been found.

As previously mentioned, available measured or computed data is rather scarce, and as a consequence we are forced to rely on limited number of test cases in order to validate this work.

The first validation attempt relied upon a power conservation test. In this way, we have verified that when the materials involved are lossless, the net power flow from the unit cell is zero.

The power dissipated in the basic cell can be derived from the knowledge of the scattering coefficients and of the amplitude of the incident plane wave E_0, supposed to be real, as

$$-\tfrac{1}{2}\,\Re e\left\{ \oint_{S_c} (\vec{E} \times \vec{H}^*) \cdot \hat{\rho}\, dS \right\} = -P_{ss} - P_{si} = \text{total power dissipated} \tag{34}$$

where

$$P_{ss} = 2D_z \sum_{m=-\infty}^{\infty} \sum_{n=\eta_n>0-\infty}^{\infty} \frac{1}{k_{\rho_n}^2} (\omega\mu_0 |a_{mn}^{\mathrm{TE}}|^2 + \omega\epsilon_0 |a_{mn}^{\mathrm{TM}}|^2) \qquad \eta_n > 0 \tag{35a}$$

$$P_{si} = 2D_z \frac{E_0}{k_{\rho_0}} \sum_{m=-\infty}^{\infty} \Re e\left\{ (-j)^m \chi \frac{k_0}{\omega\mu_0} a_{m0}^{\mathrm{TM}} + (-j)^m (1-\chi) a_{M0}^{\mathrm{TE}} \right\} \tag{35b}$$

and $\chi = 0$ for TE_z incidence or $\chi = 1$ for TM_z incidence.

It might be assumed that one can look at the numerically evaluated power dissipated in the lossless structure also in order to estimate the error introduced by a less than optimum mesh or perhaps to investigate the tolerance set for the conjugate gradient solver. However, we have established that this quantity may nevertheless give us a very small net power dissipation even when an inappropriate choice of either mesh or tolerance is made, making the latter difficult to identify. Now, the term P_{ss}, appearing in (34), is related to only the components of the scattered field while P_{si} is the mutual interaction term of the incident and scattered field components. Furthermore, these two terms are related to the real part of the equivalent blockage width W_{eq} [7] as

$$P_{ss} = -P_{si} = \frac{k_{\rho_0} D_z}{\omega\mu_0} |E_0|^2 \Re e\{W_{\mathrm{eq}}\} \tag{36}$$

and, therefore, they are also related to the real part of the induced field ratio IFR [2] being $W_{\mathrm{eq}} = -W \cdot \mathrm{IFR}$, where W is the width of the cylinder orthogonal to the plane of incidence.

If the structure is lossless, for any numerical result, the two terms P_{ss} and P_{si} provide two different estimates of the same quantity and their relative error can indicate the uncertainty in the evaluation of the equivalent blockage width.

Although the power consevation test is very useful to check whether the program code works correctly or not, it is a necessary but not sufficient test if we want to investigate the suitability of the mesh or the accuracy of the conjugate gradient solver solution [18].

The convergence of the method has been tested by analyzing simple structures for which an analytical solution is known. In particular, we have studied the scattering from cylinders which

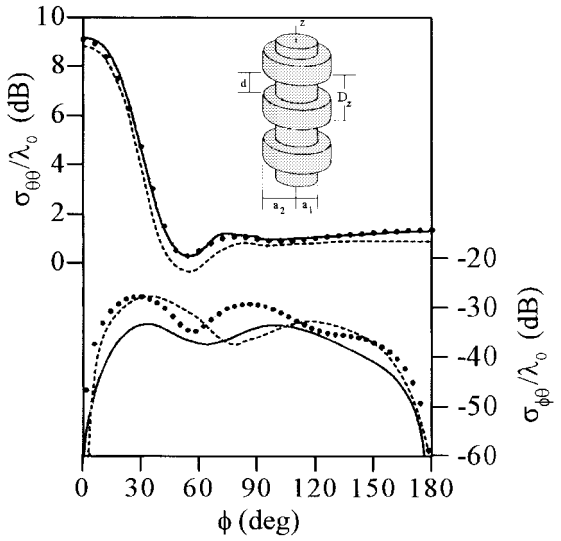

Fig. 3. Co-polar (upper curves) and cross-polar (lower curves) scattering width for a plane wave, with TM_z polarization, impinging at an angle $\theta^i = 85°$ $(a_1 = 0.4\lambda_0, a_2 = 0.5\lambda_0, D_z = 0.3\lambda_0, d = 0.2\lambda_0)$. FEM solution (solid symbols), mode matching solution (continuous line), method-of-moment solution (dashed line).

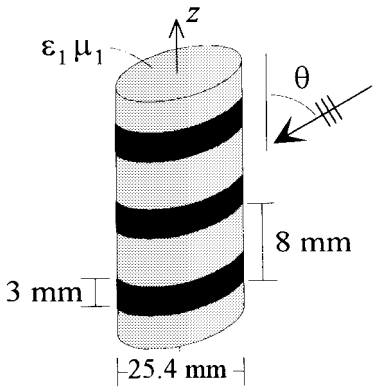

Fig. 4. Geometry of the structure relatives to the results in Figs. 5 and 6.

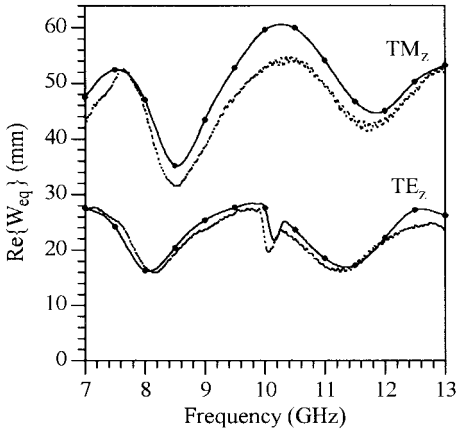

Fig. 5. Real part of the equivalent blockage width versus frequency for a plane wave impinging at an angle $\theta^i = 60°$ for both TM_z and TE_z polarizations: FEM solution (solid line), measurements shown in [20] (dotted line).

are uniform in the z-direction and made up from concentric dielectric layers of circular cross section. Such a cylinder can be considered as a periodic structure with arbitrary period D_z. In all the simulations the evaluated scattering coefficients a_{mn}^{TE} and a_{mn}^{TM} agreed with the analytical ones up to the fourth decimal digit when we have employed elements with largest side smaller than one third of the wavelength in the material considered. Furthermore, we have analyzed an infinitely long cylinder of circular cross section periodically loaded with by infinitely thin metallic annular rings. A good agreement for the results of our finite-element solution and an analytical solution has been reported already for this somewhat idealized structure [11]. Results for more practical structures are now reported below.

Fig. 3 shows the co-polar (upper curves) and cross-polar (lower curves) scattering width (two-dimensional RCS) for a plane wave, with TM_z polarization, impinging at an angle $\theta^i = 85°$ on a circular conducting cylinder of radius $a_1 = 0.4\lambda_0$ loaded with conducting disks of radius $a_2 = 0.5\lambda_0$. The periodicity of the structure is $D_z = 0.3\lambda_0$ and the spacing between discs is $d = 0.2\lambda_0$. In the figure, the solution obtained from our FEM code (solid symbols) is compared with that evaluated from a mode-matching method (continuous line) described in [10] and a method-of-moment solution (dashed line) [19]. The agreement can also be considered good for the cross-polar component because of the very low value of the scattering width.

Additionally, we have considered the scattering of a dielectric circular cylinder $(\epsilon_r = 2.1)$ of radius $a = 12.7$ mm loaded with metallic bands having width of 3 mm and a periodicity $D_z = 8$ mm, as sketched in Fig. 4.

Fig. 5 shows the real part of the equivalent blockage width in the range from 7 to 13 GHz when a plane wave impinges on the cylinder at an angle $\theta^i = 60°$. In particular, the results of our analysis (solid line),[1] for both TM_z and TE_z polarizations, are compared with the measurements (dotted line) shown in [20].

It is worth noting that in the TE_z case, a discontinuity is present close to 10 GHz in both the experimental and the numerical results. This frequency coincides with the cutoff frequency of the TE_{01} mode of a metallic circular waveguide filled with the same dielectric as the strip-loaded cylinder. This behavior is more evident in Fig. 6, which shows the real part of the equivalent blockage width for a case where the plane wave impinges orthogonally on the structure of Fig. 4. In particular, the three discontinuities present in the TE_z curve at about 7.8, 9.6, and 10.8 GHz can be related to the cutoff frequency of the mode TE_{21} $(f_c = 7.92$ GHz), TE_{01} $(f_c = 9.94$ GHz), TE_{31} $(f_c = 10.89$ GHz), respectively. On the other hand, no form of discontinuity has been observed for the TM_z case even where TM modes can propagate in the equivalent metallic circular waveguide in the frequency range analyzed in Figs. 5 and 6. The TE_z-plane wave incident orthogonally upon the "cage structure" circular waveguide of Fig. 4 has a z-directed magnetic field which evidently couples to the longitudinal z-

[1]Note that in Figs. 5, 6, 8, and 9, dots are added to the lines representing finite-element solutions purely for clarity in distinguishing the latter from the experimental measurements. The frequency step employed was 0.1 GHz (and where necessary, even smaller).

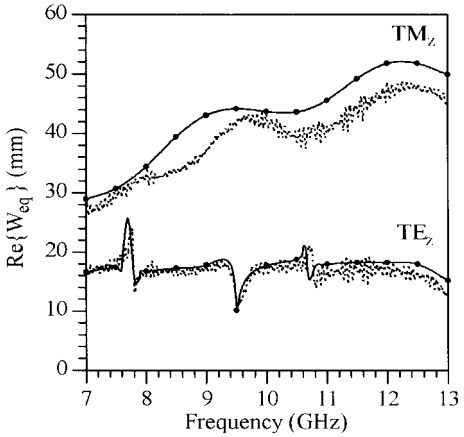

Fig. 6. Real part of the equivalent blockage width versus frequency for a plane wave impinging at an angle $\theta^i = 90°$ for both TM_z and TE_z polarizations: FEM solution (solid line), measurements (dotted line).

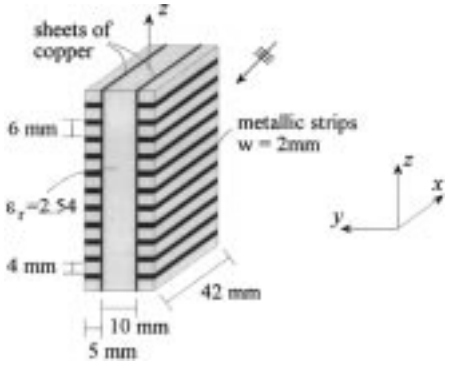

Fig. 7. Geometry of the structure analyzed in Figs. 8 and 9.

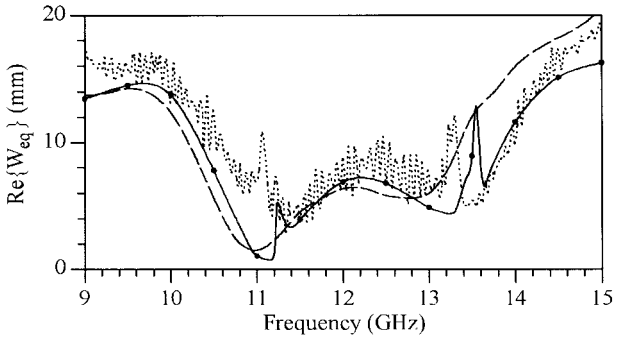

Fig. 8. Real part of the equivalent blockage width versus frequency for an orthogonally incident plane wave having TE_z polarization: FEM solution (solid line), measurements (dotted line) [7], approximate solution (dashed line) [7].

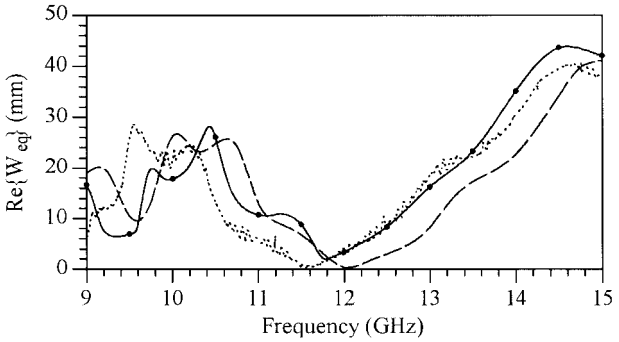

Fig. 9. Real part of the equivalent blockage width versus frequency for an orthogonally incident plane wave having TM_z polarization: FEM solution (solid line), measurements (dotted line) [7], approximate solution (dashed line) [7].

component of the magnetic field existing inside the waveguide at the walls for TE waveguide modes, particularly at the cutoff frequencies. However, the orthogonally incident TM_z-plane wave substitutes instead a z-directed electric field whereas the corresponding z-directed electric fields for the TM waveguide modes of course vanish at the waveguide walls, so in this instance there is minimal coupling. Thus discontinuities in the TM_z blockage width curve at the equivalent circular waveguide TM cutoff frequencies are not expected.

In Fig. 7, a more complex strut which can be used for dual polarization is shown. In particular, it consists of a dielectric cylinder $(\epsilon_r = 2.54)$ periodically loaded with metallic strips across the strut. The strips cover the front and the back sides of the outer dielectric coating, but do not cover the apertures of the parallel-plate waveguide constituted by the interior metallic sheets.

Figs. 8 and 9 show the real part of the equivalent blockage width versus frequency for incident plane waves having TE_z and TM_z polarization, respectively. The plane wave is supposed propagating along the negative direction of the x-axis and impinging orthogonally on the shorter side of the rectangular cross-section cylinder. For both cases, the equivalent blockage width obtained with the proposed FE method (solid line) is compared with the measured data reported in [7] (dotted line) and an approximate solution also reported in [7] (dashed line).

Although some discrepancies between calculated and measured equivalent blockage width can be observed, mainly due to the tolerances in the manufacturing of the strut as stated in [7], it is worth noting that the two discontinuities appearing in the measurements for the TE_z polarization (Fig. 8), close to 11 and 13.2 GHz, can be reproduced by the proposed method, even if with a little frequency shift. Accordingly, these discontinuities are not measurement errors but can be related to modes TE_{50} $(f_c = 11.2$ GHz) and TE_{60} $(f_c = 13.45$ GHz) in the rectangular waveguides, of dimensions 42 $\times$ 5 mm, each formed by the metallic strips and one of the two parallel plates.

To confirm that these discontinuities relate to a guidance effect we have further analyzed a structure similar to Fig. 7 but now with the space contained by each metallic strip and the sheet of copper filled with a perfect electric conductor. Thus, this new structure prevents any longitudinal propagation of the field in the two lateral parts. Fig. 10 shows the real part of the simulated equivalent blockage width versus frequency for a TE_z polarized plane wave orthogonally incident upon the new strut geometry (solid line) compared with the previous results for the geometry of Fig. 7 (dashed line). It may be noted that for the actual geometry the discontinuities disappear, as expected, and for the remaining frequencies only a slight difference between the two curves can be observed.

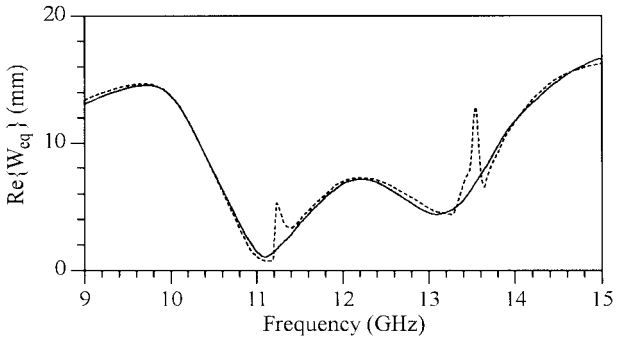

Fig. 10. Real part of the equivalent blockage width versus frequency for an orthogonally incident plane wave having TE_z polarization: FEM solution for the same structure as Fig. 7 but having the space contained by each metallic strip and the sheet of copper filled with perfect electric conductor (solid line), FEM solution for the strut of Fig. 7 (dashed line).

IV. Conclusions

A finite element/boundary element formulation has been worked out to apply to the scattering of a plane wave incident generally upon an arbitrary strut which is spatially periodic in the longitudinal direction. The inhomogeneous region constituting the strut and its immediate surroundings is modeled by applying the finite-element method to a circular cylindrical unit cell discretized into Crowley–Silvester curvilinear hexahedral covariant projection vector finite elements. The surface integrals to be associated with such a formulation cancel over the two periodic ends of the cell, while the corresponding integral over the curved side-boundary is made compatible with an infinite series of cylindrical harmonics representing the incident plane wave and the resulting scattered Floquet harmonics. Requiring the tangential components of both electric and magnetic field to be continuous through the circular cylindrical cell boundary results in the amplitudes of the Floquet harmonics to be determined.

The hybrid finite element/boundary element code resulting from this formulation has been verified in a number of different ways. A procedure testing that the incident wave and the set of scattered waves are together consistent with the rules of power conservation has been applied and found useful during program development. However, it should be noted that the confirmation of power conservation relating to any given numerical simulation is only a necessary, but not sufficient, condition that the solution should accurately represent the physical situation being modeled. For instance, with a grossly coarse discretization or an inadeqate convergence of the conjugate gradient solver, the power conservation test may still record an apparently satisfactory result. At the next level, it was verified that the code reproduced known analytical results for the scattering of waves from axially uniform, layered cylindrical cylinders and from a circular conducting cylinder periodically loaded with infinitely thin annular rings. For the axially uniform rod this was done on the basis that such a rod may be considered to repeat with arbitrary spatial "periodicity" and analyzed as such.

For further verification of the code it was necessary to check against experimental results carried out and published by other workers. This was done satisfactorily for a corrugated circular conducting cylinder and for a dielectric rod periodically loaded with metallic bands. Finally, a much more complex structure of rectangular cross section was analyzed. This was essentially a dielectric-spaced strip line but with the strip conductors coated on the outside with the same dielectric, that coating further being periodically loaded with metallic strips without short-circuiting the transmission line. In this case, bearing in mind the difficulties both in accurately fabricating such a structure and in carrying out the scattering measurements, the agreement obtained between the computed and practical results was considered to be acceptable.

Acknowledgment

The authors wish to thank Prof. J. P. Webb, of McGill University, for providing the basic routines of covariant-projection edge elements, and to thank Prof. P.-S. Kildal, of Chalmers University, for helpful discussions and for providing measurements results.

References

[1] J. Ruze, "Feed support blockage loss in parabolic antennas," *Microwave J.*, vol. 11, no. 12, pp. 76–80, 1968.
[2] W. V. T. Rush, J. Appel-Hansen, C. A. Klein, and R. Mittra, "Forward scattering from square cylinders in the resonance region with application to aperture blockage," *IEEE Trans. Antennas Propagat.*, vol. 24, pp. 182–189, Mar. 1976.
[3] P.-S. Kildal, E. Olsen, and J. A. Aas, "Loss, sidelobes, and cross polarization caused by feed-support struts in reflector antennas: Design curves," *IEEE Trans. Antennas Propagat.*, vol. 36, pp. 182–190, Feb. 1988.
[4] P.-S. Kildal, "Artificially soft and hard surfaces in electromagnetics," *IEEE Trans. Antennas Propagat.*, vol. 38, pp. 1537–1544, Oct. 1990.
[5] T. Satoh, S. Endo, N. Matsunaka, S. Betsudan, T. Katagi, and T. Ebisui, "Sidelobe level reduction by improvement of strut shape," *IEEE Trans. Antennas Propagat.*, vol. 32, pp. 698–705, July 1984.
[6] P.-S. Kildal, C. Luptovics, and O. Forslund, "Hard struts reduce aperture blockage in axisymmetric reflector antennas," in *IEEE AP-S Int. Symp.*, Chicago, IL, July 1992, pp. 1145–1148.
[7] P.-S. Kildal, A. Kishk, and A. Tengs, "Reduction of forward scattering from cylindrical objects using hard surfaces," *IEEE Trans. Antennas Propagat.*, vol. 44, pp. 1509–1520, Nov. 1996.
[8] T. C. Rao, "Plane wave scattering by a corrugated conducting cylinder at oblique incidence," *IEEE Trans. Antennas Propagat.*, vol. 36, pp. 1184–1188, Aug. 1988.
[9] C. Eftimiu, "Electromagnetic scattering by rough conducting circular cylinders—II: Axial corrugation," *IEEE Trans. Antennas Propagat.*, vol. 36, pp. 659–663, May 1988.
[10] G. Manara, G. Pelosi, A. Monorchio, and R. Coccioli, "Plane-wave scattering from cylinders with transverse corrugations," *Electron. Lett.*, vol. 31, no. 6, pp. 437–438, Mar. 1995.
[11] A. Freni, "Scattering from a dielectric cylinder axially loaded with periodic metallic rings," *Proc. Inst. Elec. Eng.—Microw. Antennas Propagat.*, vol. 143, no. 3, pp. 233–237, June 1996.
[12] J. P. Webb and R. Miniowitz, "Analysis of 3-D microwave resonators using covariant-projection elements," *IEEE Trans. Microwave Theory Tech.*, vol. 39, pp. 1895–1899, Nov. 1991.
[13] T. Cwik, "Coupling into and scattering from cylindrical structures covered periodically with metallic patches," *IEEE Trans. Antennas Propagat.*, vol. 38, pp. 220–226, Feb. 1990.
[14] P. P. Silvester and R. L. Ferrari, *Finite Elements for Electrical Engineers*, 3rd ed. Cambridge, U.K.: Cambridge Univ. Press, 1996.
[15] R. L. Ferrari, "Finite element solution of time-harmonic modal fileds in periodic structures," *Electron. Lett.*, vol. 27, no. 1, pp. 33–34, Jan. 1991.
[16] ——, "Spatially periodic structures," in *Finite Element Software for Microwave Engineering*, T. Itoh, G. Pelosi, and P. Silvester, Eds. New York: Wiley, 1996, pp. 25–52.
[17] J. A. Stratton, *Electromagnetic Theory*. New York: McGraw Hill, 1941.

[18] C. Mias, "Finite element modeling of the electromagnetic behavior of spatially periodic structures," Ph.D. dissertation, Cambridge Univ., Cambridge, U.K., 1995.
[19] G. B. Giambiasi, "Analisi della reirradiazione elettromagnetica da parte di superfici cilindriche corrugate," Laurea degree dissertation, Univ. Pisa, Pisa, Italy, 1995.
[20] A. Kishk and P.-S. Kildal, "Asymptotic boundary conditions for strip-loaded scatterers applied to circular dielectric cylinders under oblique incidence," in *IEEE AP-S Int. Symp.*, Baltimore, MD, July 1996, pp. 860–863.

Angelo Freni (S'90–M'91) was born in Florence, Italy, in 1959. He received the doctor degree in electronic engineering from the University of Florence, Florence, Italy, in 1987.

In 1990, he joined the Department of Electronic Engineering of the University of Florence as an Assistant Professor. Since 1994, he has been also an Adjunct Professor at the University of Pisa, Pisa, Italy. His research interest include radar systems, radiowave propagation, and numerical and asymptotic methods in electromagnetic scattering and radiation problems. In particular, part of his research concerned the extension and the application of the finite-element method to the electromagnetic scattering from periodic structures and to the electromagnetic interaction with moving media.

Christos Mias (M'96) received the B.Eng. (honors) degree in electronic and communication engineering from Bath University, Bath, U.K., in 1991. In 1995, he received the Ph.D. degree from Cambridge University, Cambridge, U.K.

From 1995 until 1997 he worked as a Research Fellow at Birmingham University, Birmingham, U.K. In 1997, he joined the Nottingham Trent University, Nottingham, U.K., as a Lecturer. His research interests include the application of the finite-element method in the modeling of periodic structures.

Ronald L. Ferrari was born in Romford, U.K. in 1930. He graduated in mathematics from Imperial College of Science and Technology, University of London, London, U.K., in 1950, and was awarded the Diploma of Imperial College in 1951.

After commissioned service in the Royal Air Force doing radar operational research, in 1956 he joined the Hirst Research Centre of GEC Ltd, Wembley, U.K., researching in semiconductors and microwaves. He was appointed Lecturer in Engineering at Cambridge University in 1965 and Fellow of Trinity College, Cambridge in 1966, being awarded the Sc.D. higher doctorate of Cambridge University in 1994, and retiring from teaching in 1997. He has held visiting posts at Cornell, McGill, and Florence Univerities. In addition to papers on solid-state physics, microwaves, radioecho sounding, and numerical electromagnetics, his publications include the book *Finite Elements for Electrical Engineers* (with the late P. P. Silvester) and a textbook on electromagnet fields.

Dr. Ferrari is a Fellow of the Institution of Electrical Engineers, London, U.K.